



PERGAMON

Atmospheric Environment 36 (2002) 511–517

**ATMOSPHERIC  
ENVIRONMENT**

www.elsevier.com/locate/atmosenv

Short communication  
**Effects of wind shear on pollution dispersion**

Chris J. Walcek\*

*State University of New York, Albany, NY 12203, USA*

Received 9 February 2001; accepted 13 July 2001

**Abstract**

Using an accurate numerical method for simulating the advection and diffusion of pollution puffs, it is demonstrated that point releases of pollution grow into a shape reflecting the vertical wind shear profile experienced by the puff within a time scale less than 4 h. For distances beyond several 10 s of kilometers from a release point, shear-related dispersion effects are probably the dominant mechanism affecting the area and magnitude of surface impacts. For assessing long-range pollutant dispersion, the common assumption that pollutants disperse as horizontally spherical “puffs” in the atmosphere is inherently inaccurate since shear-induced horizontal spreading of pollution is not a homogeneous “turbulent-like” diffusion process. A Lagrangian puff model can simulate an area impacted by a pollution puff only if larger shear-dependent horizontal puff dispersions are assumed. However, even if impacted areas are reasonably simulated, peak concentrations will be severely underestimated since atmospheric puffs influenced by even small amounts of wind shear are nonspherical. If horizontal dispersion coefficients in a Lagrangian puff model are adjusted so that peak concentrations are correctly simulated, then the calculated pollution impact area will be severely skewed. In shear environments, no choice of horizontal dispersion coefficients in a single-puff Lagrangian model will yield reasonable correlations with puffs that are skewed into nonspherical shapes by atmospheric wind shear. © 2002 Elsevier Science Ltd. All rights reserved.

*Keywords:* Air pollution; Pollution dispersion; Gaussian dispersion; Trajectories; Lagrangian; Puff models; Long-range transport; Trajectory; Plume

**1. Introduction**

Simulations of atmospheric pollution have generally been approached from two modeling perspectives. Eulerian models numerically integrate fundamental advection- and diffusion-concentration tendency equations forward in time over a multi-dimensional grid encompassing a domain of interest. In contrast, Lagrangian models calculate a trajectory path that is assumed to describe the movement of the “center” of an individual puff, and diffusion independently spreads the pollutant away from the puff center.

One of the recognized limitations of Lagrangian puff models is the behavior of transport and dispersion in

environments where wind speeds or directions change over the spatial extent of a puff. Under these conditions, the specification of radially symmetric dispersion relative to the puff center becomes inaccurate. Some Lagrangian models allow individual puffs to “split” into multiple “daughter” puffs to crudely account for shear-related effects (e.g. Draxler and Hess, 1998). However, pollution is still assumed to diffuse radially away from each puff center, and the methodologies used to “spawn” puffs are ad hoc and are difficult to explicitly validate. Other more sophisticated Lagrangian approaches utilize increasingly complex puff concentration formulations, assuming more complex wind patterns around a puff (e.g. Sykes and Henn, 1995). However, even for these more complex puffs, only relatively simple wind deformations are considered, and with more complex and realistic winds, the puff formulations become computationally unwieldy.

\*Tel.: +1-518-437-8720; fax: +1-518-437-8758.

*E-mail address:* walcek@asrc.cestm.albany.edu  
(C.J. Walcek).

In this study, simulations are carried out under idealized, but not unrealistic, atmospheric conditions to demonstrate the effects of wind shear on the transport and dispersion of a pollution puff. In Section 2, the numerical methods of an explicit “Eulerian puff” model are described. In Section 3, a “Lagrangian puff” formulation is presented. These two models are compared in Section 4 using observed winds, with and without vertical shear.

## 2. Eulerian puff model

An individual puff of pollution is simulated, by numerically integrating the three-dimensional advection–diffusion equation forward in time ( $t$ ):

$$\frac{\partial c}{\partial t} = -\frac{\partial(uc)}{\partial x} - \frac{\partial(vc)}{\partial y} + \frac{\partial}{\partial x}\left(\frac{\partial(K_h c)}{\partial x}\right) + \frac{\partial}{\partial y}\left(\frac{\partial(K_h c)}{\partial y}\right) + \frac{\partial}{\partial z}\left(\frac{\partial(K_z c)}{\partial z}\right), \quad (1)$$

where  $c$  is the concentration of a pollutant in air. Horizontal transport is specified using  $u$  (west-to-east,  $x$ -direction) and  $v$  (south-to-north,  $y$ -direction) winds. Mean vertical advection, which is usually small in the atmospheric planetary boundary layer (PBL), is neglected. Turbulence is quantified using horizontal and vertical Fickian diffusion coefficients  $K_h$  and  $K_z$ . For this study,  $K_h$  and  $K_z$  are horizontally uniform and constant in time, but can vary with height ( $z$ ), and are set to zero at the PBL top ( $Z_{\text{pbl}}$ ), and at the surface ( $z = 0$ ). While these assumptions are probably not appropriate for large domains or long-transport distances, it will be shown that even under these simplified conditions, substantial deviations from Lagrangian puff theories arise when wind speeds change vertically.

This Eulerian advection and diffusion model uses a 60-s time step, and changes in concentration due to horizontal advection are calculated first, followed by horizontal and vertical diffusion calculations. Advection is numerically calculated using the Walcek (2000) sharpened piecewise linear algorithm. Diffusion is simulated using a forward-time, centered space flux-form finite difference approximation.

For all simulations, the domain is defined as a late-afternoon summertime PBL, 2400 m thick. The PBL is vertically divided into 12 layers ( $\Delta z = 200$  m). The domain sizes in the west–east and south–north directions are 80 and 120 grid cells, and initially  $\Delta y = \Delta x = 500$  m. At time  $t = 0$ , a mass of pollution is placed in one model grid cell 400–600 m above the surface, near the upwind edge of the domain. For all simulations, a background concentration of  $1 \mu\text{g m}^{-3}$  is specified, and the mass of pollution added ( $Q$ ) is  $4.9995 \times 10^{11} \mu\text{g}$ , yielding an initial concentration of

$10^4 \mu\text{g m}^{-3}$  in the emission cell. Background concentrations ( $1 \mu\text{g m}^{-3}$ ) are specified as inflow boundary conditions. During the simulation, if the edge of the puff impinges on the edge of the domain, the domain size is doubled in the downwind direction, and concentrations are averaged into the expanded cells so that a larger domain is simulated. All the simulations follow puff dispersion and advection for 4 h.

## 3. Lagrangian puff model

The Eulerian model described above is compared with an alternate Lagrangian parcel-trajectory model, which follows standard assumptions employed by classical puff dispersion models (e.g. Shannon, 1981; Draxler and Taylor, 1982). For a pollution puff initially released at a point and diffusing in an environment of spatially constant winds and diffusivities, limited vertically by the surface ( $z = 0$ ) and PBL top, the concentration around the puff center can be calculated using

$$c = c_{\text{back}} + \frac{Q}{(2\pi)^{1.5} \sigma_h^2 \sigma_z} \exp\left(\frac{-(x - x_c)^2}{2\sigma_h^2} - \frac{(y - y_c)^2}{2\sigma_h^2}\right) \times \left[ \exp\left(\frac{-(z - z_e)^2}{2\sigma_z^2}\right) + \exp\left(\frac{-(z + z_e)^2}{2\sigma_z^2}\right) + \exp\left(\frac{-(z - 2Z_{\text{pbl}} - z_e)^2}{2\sigma_z^2}\right) + \exp\left(\frac{-(z - 2Z_{\text{pbl}} + z_e)^2}{2\sigma_z^2}\right) + \exp\left(\frac{-(z + 2Z_{\text{pbl}} - z_e)^2}{2\sigma_z^2}\right) + \exp\left(\frac{-(z + 2Z_{\text{pbl}} + z_e)^2}{2\sigma_z^2}\right) \right], \quad (2)$$

where  $c_{\text{back}}$  is a background concentration and  $Q$  is the mass of pollutant in the puff. The center of the puff is located at  $x_c$  and  $y_c$ , and  $z_e$  is the puff emission height (500 m).  $\sigma_h$  and  $\sigma_z$  are the horizontal and vertical dispersion of the concentration distribution around the puff center. The six  $z$ -dependent exponential terms in Eq. (2) are vertical reflecting terms required since diffusion is not allowed above the top of the PBL or below the surface.

The location of the puff center ( $x_c, y_c$ ) is calculated following a trajectory:

$$x_c(t + \Delta t) = x_c(t) + u_p \Delta t, \\ y_c(t + \Delta t) = y_c(t) + v_p \Delta t, \quad (3)$$

where  $\Delta t$  is the time step of the trajectory calculation, and wind speeds moving the puff,  $u_p$  and  $v_p$ , are mass-weighted averages of the winds encountered by the puff.

According to Fickian diffusion theory, the horizontal and vertical dispersion distance  $\sigma$  of pollutants away from a puff center is

$$\sigma = \sqrt{2Kt}, \quad (4)$$

where  $t$  is the time since the release of the pollution at a point, related to the downwind distance  $d$  ( $t = d/u$ ). If Eq. (4) is used for calculating  $\sigma_h$  and  $\sigma_z$ , Eq. (2) represents an analytical solution to the three-dimensional advection–diffusion Eq. (1).

Diffusion coefficients ( $K$ ) in the lower PBL can be reasonably represented using mixing-length/similarity theory of atmospheric turbulence, but when  $K$ s quantified in this manner are used to estimate puff or plume dispersion, gross discrepancies between theoretical and measured dispersion are observed. In particular, Eq. (4) implies that the size of a plume should grow as the square root of the downwind distance from the release point ( $\sigma_h \sim d^{0.5}$ ), while measurements usually show significantly greater dispersion that increases in proportion to appreciably greater powers of downwind distance ( $\sigma_h \sim d^{0.7-1.5}$ ). Most dispersion models empirically specify horizontal dispersions  $\sigma$  to be consistent with a large body of dispersion measurements, and are not based on Fickian diffusion principles. It is generally recognized that shear-related effects are the dominant factors enhancing dispersion, relative to the purely turbulent diffusive tendencies (e.g. Smith, 1965; Randerson, 1972).

#### 4. Results

The Eulerian puff model is first validated using simplified constant winds and diffusion conditions for which analytical solutions to the puff advection–diffusion equation are available. This idealized simulation validates the accuracy of the numerical approximations used by the Eulerian model. Another calculation is then performed using atmospheric winds measured during a late summertime afternoon.

##### 4.1. Idealized dispersion: no shear

For this evaluation test, horizontal and vertical diffusion coefficients  $K_h$ ,  $K_z$  are everywhere  $100 \text{ m}^2 \text{ s}^{-1}$  except at the PBL top ( $Z_{\text{pbl}} = 2400 \text{ m}$ ) and at the surface ( $z = 0$ ), where  $K_h = K_z = 0$ . Diffusion coefficients of this magnitude are, approximately, consistent with similarity theory flux–gradient relationships derived using observed surface roughness, late-afternoon sensible heat fluxes and measured surface layer winds. The average PBL wind speed, taken from the following atmospheric test ( $\bar{u} = 5.217 \text{ m s}^{-1}$ ) is split into horizontally constant west–east and south–north components:  $u = 2.781$  and  $v = 4.414 \text{ m s}^{-1}$ . Under these idealized conditions, Eq. (2) with  $\sigma = \sqrt{2Kd/\bar{u}}$  represents an analytical

solution to Eq. (1) that can be directly compared with the numerically approximate Eulerian calculations.

Fig. 1 shows surface concentrations ( $0 < z < 200 \text{ m}$ ) during each hour for 4 h after emission. The maximum surface concentrations calculated by the Eulerian and Lagrangian models are tabulated in the figure. Fig. 2 shows a vertical profile of the north–south, 120 km-long average of the concentrations around the puff shown in Fig. 1, 4 h after release. Figs. 1 and 2 demonstrate that the numerical approaches used by this Eulerian model are reasonable, showing that the Eulerian model can accurately simulate transport and dispersion of a point puff of pollution in the atmosphere for distances of over 75 km downwind of the release location, even when winds are directed diagonally across the grid.

##### 4.2. Simulations with observed PBL winds

The models described above are now used to simulate the transport and dispersion of a puff of pollution using atmospheric winds that vary vertically. Winds are taken

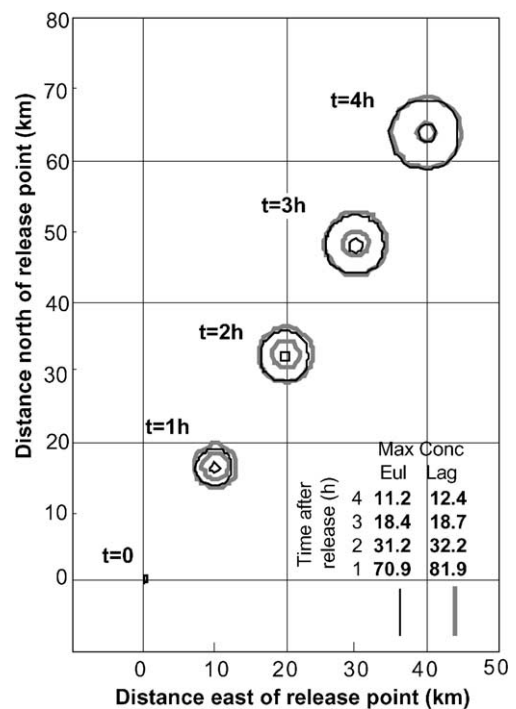


Fig. 1. Surface concentrations ( $\mu\text{g m}^{-3}$ ) above background levels at hourly intervals within a puff of pollution initially emitted 0.5 km above the surface in a 2.4 km deep PBL, advected with constant winds and diffused by uniform turbulence. Gray contours are exact analytical Lagrangian solutions to the translated and reflecting puff-diffusion equation. Black contours are calculated using the Eulerian model. Contours are 2% and 80% of the peak Eulerian concentrations.

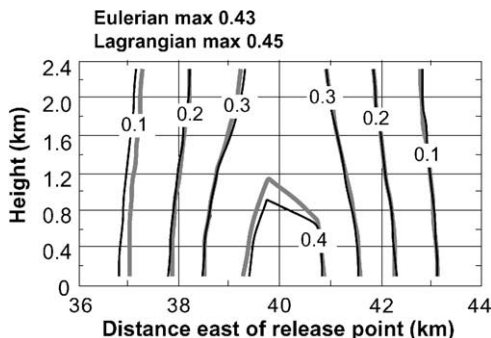


Fig. 2. Vertical profile of 120 km north-south average of concentrations above the background around a puff, 4h after release, for the conditions shown in Fig. 1. Exact Lagrangian calculations shown as gray contours. Eulerian concentrations are shown as solid lines.

from a routine 0 UT 14 June 2000 Albany, NY radiosonde launched about 1 h before local sunset on a relatively clear, sunny and moderately windy afternoon. Fig 3 shows a hodograph of wind vectors at heights progressing up from the surface. In the lower PBL, winds are out of the south, while in the upper PBL, winds veer to a west-to-easterly flow. Potential temperatures measured with the sounding were approximately constant up to 2.2 km above the surface, where a potential temperature inversion was encountered. Surface temperatures and stability analysis showed that the height of the PBL containing turbulence was approximately 2.4 km.

For this atmospheric simulation, diffusion coefficients  $K_h$  and  $K_z$  are equal, and are specified to increase linearly with height from zero at the surface to  $100 \text{ m}^2 \text{ s}^{-1}$  at  $z = 0.36 \text{ km}$ . Above 0.36 km, diffusion coefficients are constant between 0.36 and 2.16 km. Above 2.16 km, diffusion coefficients linearly decrease from the mid-PBL values to zero at the top of the PBL. For the Lagrangian model, dispersion about the puff center is specified using Eq. (4), although additional calculations are performed using a wide range of  $\sigma_h$ .

Fig. 4 shows surface-level calculations of the shape and peak concentration of Lagrangian and Eulerian puff models for hourly increments after release. The area of maximum surface impact according to the Eulerian calculations remains almost due north of the release point, reflecting the impacts expected if the puff followed a trajectory using emission-height winds, which are directed to the north. In contrast, the Lagrangian puff model, using mass-weighted winds to define the trajectory, moves the puff northward initially, but after the puff becomes vertically uniformly mixed, the puff follows the mean PBL winds flowing from southwest to northeast. After 4 h, the puff is displaced about 75 km

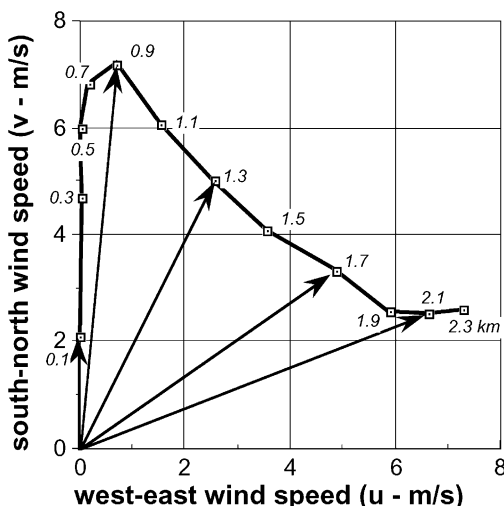


Fig. 3. Wind hodograph of the  $u$  and  $v$  wind components used in dispersion tests. Heights (km) above surface, for each wind vector, are shown near each arrow tip.

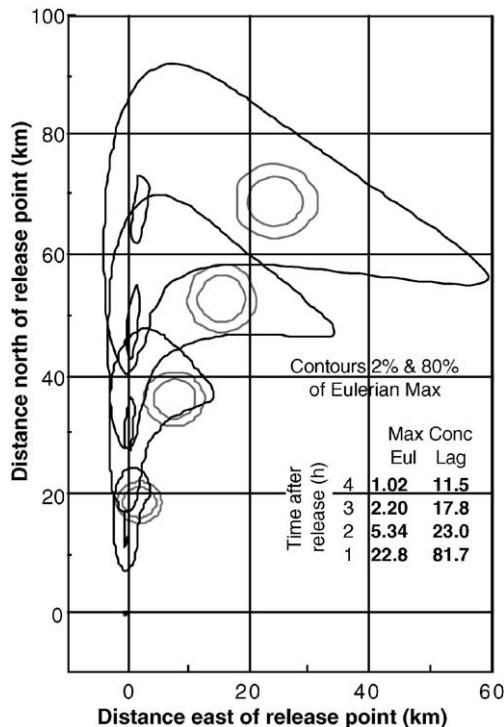


Fig. 4. Same as Fig. 1. Only observed winds shown in Fig. 3 are specified over the PBL depth. Maximum concentrations within each puff are tabulated at lower right. The contour around each puff represents 2% and 80% of the peak Eulerian puff concentration at each time.

downwind, and the location of the maximum surface impact is about 25 km east of the actual impact area. After 4 h, peak concentrations calculated from pure diffusion theory disagree by over a factor of 10 from the Eulerian model, and the puff is skewed into a shape that is similar to the crescent-shaped wind profile shown in Fig. 3. Interestingly, the centers of mass for both the Lagrangian and Eulerian puffs are identical and are located at the center of the Lagrangian position shown in Fig. 4, but according to the Eulerian model, the area of maximum surface impact is displaced appreciably from the puff center of mass. At longer times (not shown), the Eulerian model shows that the crescent-shaped puff grows and is translated by the PBL winds, but the shape remains preserved in this shear-dependent shape as long as wind speeds and directions remain fixed.

Fig. 5 shows concentrations at the base, middle, and top of the puff after 4 h. Vertical variations of the puff shape and location are fairly large according to the Eulerian model, and the Lagrangian calculations do not resemble the skewed puff distribution. In the lower PBL, winds have carried the puff to the north, but pollutants

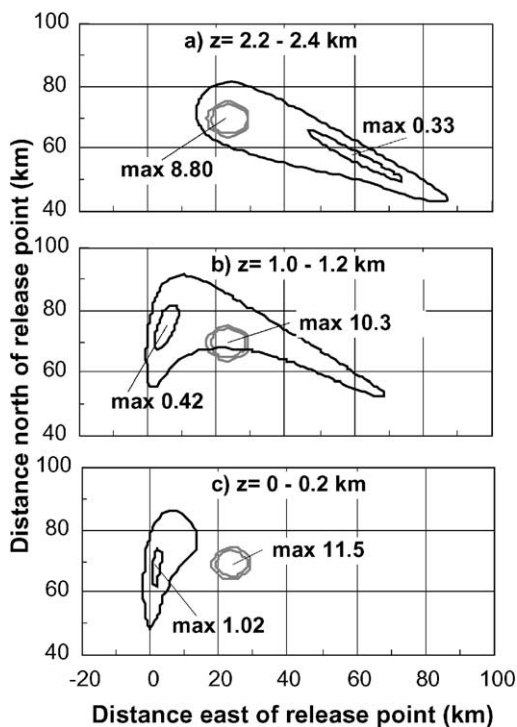


Fig. 5. Concentration distributions at three heights within the PBL for the puff shown in Fig. 4, 4 h after release. (a) Top layer of PBL; (b) middle PBL; and (c) lower PBL. Lagrangian calculations are shown as gray contours. Contours are 20% and 80% of the maximum Eulerian concentration at each layer.

have mixed upward into layers where the wind blows from southwest to northeast. In the upper PBL, pollutant is moving from west-to-east, but continues to mix downward into the northward-moving air of the lower PBL. Thus, a crescent shape develops at nearly all levels, and the location of the puff maximum concentration varies vertically, reflecting the crescent shape of the wind hodograph profile.

Parameters that are empirically adjusted within Lagrangian parcel models, are the horizontal and vertical dispersion distances,  $\sigma_h$  and  $\sigma_z$ . After 4 h, the Lagrangian puff shown in Figs. 4 and 5 uses  $\sigma_h \approx \sigma_z = 1.7$  km, calculated using Eq. (4). Classical Pasquill–Gifford (P–G) horizontal dispersions 75 km downwind of point sources range from 1 km (class “F”) to 6 km (class “A”). Increasing  $\sigma_h$  and  $\sigma_z$  has the effect of increasing the horizontal size of the Lagrangian puff while reducing the maximum concentration. Fig. 6 shows the root mean square (RMS) differences and point-by-point correlation coefficients ( $r^2$ ) between the Eulerian and Lagrangian calculations as a function of the magnitude of dispersion coefficient ( $\sigma_h$ ) used by the Lagrangian model after 4 h. No matter what value is chosen for  $\sigma_h$ , RMS differences between the models are always appreciable, and correlations with the Eulerian model are negligible, with slightly negative correlations ( $r < 0$ ) common for many choices of  $\sigma_h$ . The puff dispersion  $\sigma_h$  can be adjusted so as to minimize discrepancies with the Eulerian model, and for this case, using  $\sigma_h = 25$  km yields the smallest RMS differences.

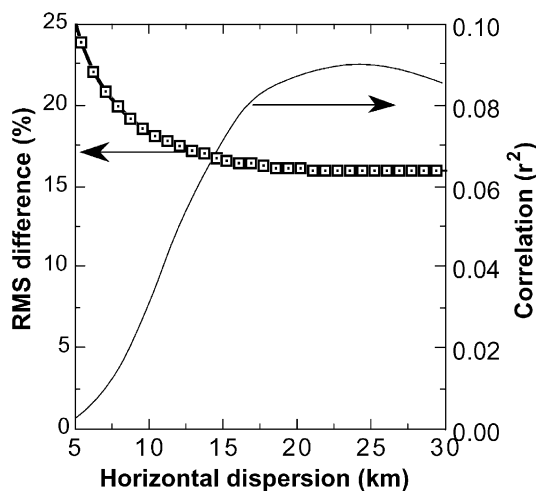


Fig. 6. Root mean square difference (box-point curve, left axis) and correlation coefficient ( $r^2$ , solid curve, right axis) between Lagrangian and Eulerian calculations for the surface puff concentrations, 4 h after release, shown in Figs. 4–5 as a function of assumed horizontal dispersion of Lagrangian puff. RMS differences normalized by range of Eulerian calculations.

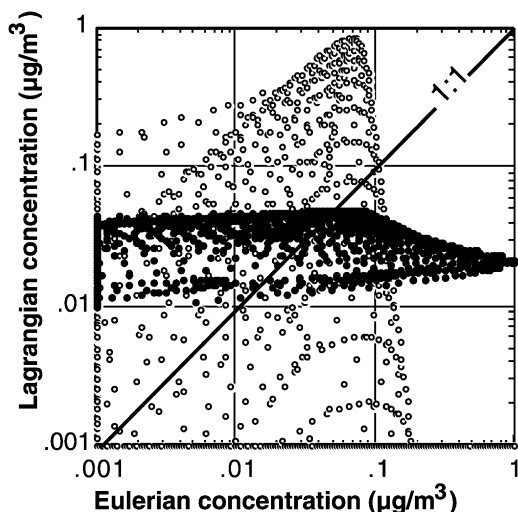


Fig. 7. Scatter diagram comparing surface concentrations shown in Fig. 4 (4 h) calculated by Eulerian and Lagrangian models. Open squares use Lagrangian horizontal dispersion, chosen so that peak concentrations calculated by Lagrangian model match Eulerian peak concentration. Solid squares use Lagrangian horizontal dispersion, chosen so that RMS errors are minimized between the two models. All the concentrations are above background, and the maximum concentration calculated by the Eulerian model at the surface is slightly greater than  $1 \mu\text{g m}^{-3}$  above background.

Fig. 7 shows a scatter diagram comparing the calculated surface concentrations at each point of the Eulerian grid, 4 h after the puff release. Calculations of the Eulerian model are compared with two choices of the “best”  $\sigma_h$ 's used by the Lagrangian model. For one simulation,  $\sigma_h = 25 \text{ km}$  is used, a value that yields the lowest RMS differences between the two models. For another Lagrangian simulation,  $\sigma_h = 5.8 \text{ km}$ , corresponding to, approximately, P–G class “A” stability conditions and the maximum surface concentrations calculated by both models agree, although the locations disagree. Fig. 7 shows that no matter what choice of  $\sigma_h$  is used by the Lagrangian model, the point-by-point comparison between the horizontally spherical Lagrangian puffs and the crescent-shaped Eulerian puff shown in Figs. 4 and 5 yields a “shotgun” scatter effect, and the Lagrangian puff model cannot reasonably simulate the skewed puff shape. The random scatter between the Lagrangian puff calculations and the crescent-shaped puff shown in Fig. 7 looks similar to the highly scattered comparison of a Lagrangian model simulation of measurements presented by Draxler (1987), where essentially negligible correlations were obtained between model calculations and measurements of several tracer releases.

Past tracer release experiments have shown that individual pollution puffs grow into complex skewed shapes (e.g. Haagenson et al., 1987). Other measurements of smoke plumes (e.g. Kinoshita, 1996) show obvious shear-induced puff distortions. In many early studies of long-range transport and diffusion, the effects of wind shear on transport and dispersion were not quantitatively assessed. In an analysis of several field studies of artificial puff releases for distances out to 100 km, Draxler (1979) evaluates a Lagrangian puff model, and the vertical wind shears in the PBL were not even reported, although significant discrepancies between a trajectory model and measurements suggest that appreciable shear was present. For example, in the Idaho Falls puff-dispersion experiment, measurements showed the puff arriving a ring of receptors 50 km downwind of a release point, a full hour before the simulated arrival time of 4 h after release, calculated using winds measured near the surface. Obviously, higher wind speeds above the surface layer would more quickly transport a puff downwind. Similarly, the Savannah River field experiment Draxler (1979) shows that 90 km downwind of a release point, the “center” of an artificially released puff passed well to the south of the projected location calculated using a Lagrangian puff-trajectory model using surface winds measured at and downwind of the release point. As shown above, minor wind-direction changes above the surface layer will move the puff in a different direction that would lead to a surface impact area appreciably displaced from the surface wind directions. Both wind speed and direction changes above the surface layer are shown here to induce the observed inconsistent puff placements downwind of release points in these past atmospheric diffusion experiments.

## 5. Conclusions

Figs. 4–7 show that, under shear conditions, the “spread” of pollution about the center of mass of a puff is markedly nonspherical in nature. All Lagrangian puff dispersion models assume radially symmetric spread of pollutant, away from the “center” of individual puffs, and it is shown here that simple adjustments of horizontal dispersion ( $\sigma_h$ ) do not lead to reasonable agreements with skewed puff concentration distributions. In order to crudely account for shear-induced effects, many Lagrangian models allow for “splitting” of a puff into multiple puffs, but the methods used cannot be readily evaluated, and it is obvious from this experiment that at least four to five superimposed “spherical” shapes would be required to mimic a skewed puff under these conditions after only 4 h.

These simulations show that individual puffs of pollution preferentially disperse in the horizontal

direction, aligned with the mean wind shear vector in the PBL. Under typical atmospheric wind conditions, extremely complex puff dispersion shapes can result that are related to the nearly ubiquitous and highly changeable shear profiles that are usually present in the PBL. For many past dispersion-field experiments, wind shear throughout the PBL was not adequately measured, and accurate vertical profiles of wind speeds and directions would be required in order to simulate dispersion of pollution in the lower troposphere.

For the atmospheric simulation shown here, the wind vector change across the vertical depth of the PBL was  $5\text{--}6\text{ m s}^{-1}$ , or  $\sim 2.5\text{ m s}^{-1}\text{ km}^{-1}$ . Shears of this magnitude are not unusual in the lower troposphere. LeMone et al. (1999) showed wind shears  $> 10\text{ m s}^{-1}\text{ km}^{-1}$ , 440 m above the surface along a tower in Oklahoma, US, during late-afternoon periods, considerably greater than the shear used here. At night, the average shear encountered in central Oklahoma, 440 m above the surface, is about  $20\text{ m s}^{-1}\text{ km}^{-1}$  according to LeMone et al. (1995). Thus the shear-related effects can be considerably greater, than shown here, under many atmospheric conditions.

#### Acknowledgements

Although the research described in this article has been funded in part by the United States Environmental Protection Agency through grant R827929010 to the Research Foundation of the State University of NY at Albany, it has not been subjected to the Agency's required peer and policy review and, therefore, does not necessarily reflect the views of the Agency and nonofficial endorsement should be inferred.

#### References

- Draxler, R.R., 1979. Modeling the results of two recent mesoscale dispersion experiments. *Atmospheric Environment* 13, 1523–1533.
- Draxler, R.R., 1987. Sensitivity of a trajectory model to spatial and temporal resolution of the meteorological data during CAPTEX. *Journal of Applied Meteorology* 26, 1577–1588.
- Draxler, R.R., Hess, G.D., 1998. An overview of the HYSPLIT-4 modeling system for trajectories, dispersion and deposition. *Australian Meteorological Magazine* 47, 295–308.
- Draxler, R.R., Taylor, A.D., 1982. Horizontal dispersion parameters for long range transport modeling. *Journal of Applied Meteorology* 21, 367–372.
- Haagenson, P.L., Kuo, Y.-H., Skumanich, M., Seaman, N.L., 1987. Tracer verification of trajectory models. *Journal of Climate and Applied Meteorology* 26, 410s–426s.
- Kinoshita, K., 1996. Observation of flow and dispersion of volcanic clouds from Mt. Sakurajima. *Atmospheric Environment* 30, 2831–2837.
- LeMone, M.A., MingYu, Z., Moeng, C.-H., Lenschow, D.H., Miller, L.J., Grossman, R.L., 1999. An observational study of wind profiles in the baroclinic convective mixed layer. *Boundary Layer Meteorology* 90, 47–82.
- Randerson, D., 1972. Temporal changes in horizontal diffusion parameters of a single nuclear debris cloud. *Journal of Applied Meteorology* 11, 670–947.
- Shannon, J.D., 1981. A model of regional long-term average sulfur atmospheric pollution, surface removal, and net horizontal flux. *Atmospheric Environment* 15, 689–701.
- Smith, F.B., 1965. The role of wind shear in horizontal diffusion of ambient particles. *Quarterly Journal of the Royal Meteorological Society* 91, 318–329.
- Sykes, R.I., Henn, D.S., 1995. Representation of velocity gradient effects in a Gaussian puff model. *Journal of Applied Meteorology* 34, 2715–2723.
- Walcek, C.J., 2000. Minor flux adjustment near mixing ratio extremes for simplified yet highly accurate monotonic calculation of tracer advection. *Journal of Geophysical Research* 105, 9335–9348.